AFRL-RV-PS-
TR-2022-0103

AFRL-RV-PS-
TR-2022-0103

BISTATIC OBSERVATIONS OF THE IONOSPHERE WITH SUPERDARN RADARS

J. M. Ruohoniemi and S. G. Shepherd

Virginia Polytechnic Institute and State University
Office of Sponsored Programs
North End Center
300 Turner Street NW, Suite 4200
Blacksburg, VA 24061-0001

07 November 2022

Final Report

AIR FORCE RESEARCH LABORATORY
Space Vehicles Directorate
3550 Aberdeen Ave SE
AIR FORCE MATERIEL COMMAND
KIRTLAND AIR FORCE BASE, NM 87117-5776

DTIC COPY

NOTICE AND SIGNATURE PAGE

Using Government drawings, specifications, or other data included in this document for any purpose other than Government procurement does not in any way obligate the U.S. Government. The fact that the Government formulated or supplied the drawings, specifications, or other data does not license the holder or any other person or corporation; or convey any rights or permission to manufacture, use, or sell any patented invention that may relate to them.

This report is the result of contracted fundamental research which is exempt from public affairs security and policy review in accordance with AFI 61-201, paragraph 2.3.5.1. This report is available to the general public, including foreign nationals. Copies may be obtained from the Defense Technical Information Center (DTIC) (http://www.dtic.mil).

AFRL-RV-PS-TR-2022-0103 HAS BEEN REVIEWED AND IS APPROVED FOR PUBLICATION IN ACCORDANCE WITH ASSIGNED DISTRIBUTION STATEMENT.

//SIGNED//	//SIGNED//
Leonard M. Berman Program Manager, AFRL/RVB	Mark E. Roverse, Chief AFRL Geospace Technologies Division

This report is published in the interest of scientific and technical information exchange, and its publication does not constitute the Government's approval or disapproval of its ideas or findings.

REPORT DOCUMENTATION PAGE

Form Approved
OMB No. 0704-0188

1. REPORT DATE *(DD-MM-YYYY)*	**2. REPORT TYPE**	**3. DATES COVERED** *(From - To)*
07-11-2022	Final Report	9 May 2018 – 26 Aug 2022

4. TITLE AND SUBTITLE
Bistatic Observations of the Ionosphere with SuperDARN Radars

5a. CONTRACT NUMBER
FA9453-18-2-0032

5b. GRANT NUMBER

5c. PROGRAM ELEMENT NUMBER
C6601F

6. AUTHOR(S)
J. M. Ruohoniemi and S. G. Shepherd[1]

5d. PROJECT NUMBER
1010

5e. TASK NUMBER
EF132904

5f. WORK UNIT NUMBER
V135

7. PERFORMING ORGANIZATION NAME(S) AND ADDRESS(ES)
Virginia Polytechnic Institute and State University
Office of Sponsored Programs
North End Center
300 Turner Street NW, Suite 4200
Blacksburg, VA 24061-0001

[1]Thayer School of Engineering
Dartmouth College
15 Thayer Dr.
Hanover, NH 03755

8. PERFORMING ORGANIZATION REPORT NUMBER

9. SPONSORING / MONITORING AGENCY NAME(S) AND ADDRESS(ES)
Air Force Research Laboratory
Space Vehicles Directorate
3550 Aberdeen Avenue SE
Kirtland AFB, NM 87117-5776

10. SPONSOR/MONITOR'S ACRONYM(S)
AFRL/RVBX

11. SPONSOR/MONITOR'S REPORT NUMBER(S)
AFRL-RV-PS-TR-2022-0103

12. DISTRIBUTION / AVAILABILITY STATEMENT
Approved for public release; distribution is unlimited (AFRL-2023-0071 dtd 05 Jan 2023).

13. SUPPLEMENTARY NOTES

14. ABSTRACT
Space systems that depend on the propagation of radio waves in the ionosphere are vulnerable to disruption owing to space weather variability of ionospheric plasma. The HF coherent radars of SuperDARN utilize refraction in the ionosphere to achieve over-the-horizon (OTH) capabilities in the pursuit of space science and technical goals. To date, the dozens of radars of SuperDARN have operated exclusively in monostatic mode. With this project SuperDARN groups at Virginia Tech and Dartmouth College have developed a bistatic capability that allows a radar in Oregon to receive the transmissions of a radar in Kansas. Numerous 3-day bistatic campaigns have been conducted over a period extending from September 2019 to March 2020. Three distinct bistatic propagation modes have been identified: direct mode, bistatic ground scatter mode, and bistatic ionospheric scatter mode. Ray tracing analysis validates the mode identification and demonstrates that with bistatic operation many more propagation paths become available for sensing the state of the ionosphere.

15. SUBJECT TERMS
ionosphere, HF, propagation, radar, bistatic

16. SECURITY CLASSIFICATION OF:			**17. LIMITATION OF ABSTRACT**	**18. NUMBER OF PAGES**	**19a. NAME OF RESPONSIBLE PERSON**
a. REPORT	**b. ABSTRACT**	**c. THIS PAGE**			Leonard M. Berman
Unclassified	Unclassified	Unclassified	Unlimited	34	**19b. TELEPHONE NUMBER** *(include area code)*

This page is intentionally left blank.

TABLE OF CONTENTS

LIST OF FIGURES

LIST OF TABLES

ACKNOWLEDGMENTS

This material is based on research sponsored by Air Force Research Laboratory under agreement number FA9453-18-2-0032. The U.S. Government is authorized to reproduce and distribute reprints for Governmental purposes notwithstanding any copyright notation thereon.

DISCLAIMER

The views and conclusions contained herein are those of the authors and should not be interpreted as necessarily representing the official policies or endorsements, either expressed or implied, of Air Force Research Laboratory or the U.S. Government.

This page is intentionally left blank.

1. SUMMARY

The space environment of the Earth both facilitates and impedes the performance of technological systems such as trans-ionospheric communications. The hazards to the space user include interruption of long-range surveillance and communications generally and degradation of links to satellites and loss of satellite tracking in particular. The HF coherent radars of the Super Dual Auroral Radar Network (SuperDARN) utilize propagation in the ionosphere to generate backscatter useful for the study of effects in the ionosphere that relate directly to space environmental variables. The radars operate in a coordinated but monostatic configuration whereby high-frequency (HF) signals scattered from ionospheric density irregularities or from the surface of the Earth return to the transmitting radar where Doppler parameters are then acquired. Virginia Tech and Dartmouth College are PI institutions for SuperDARN radar sites located in Kansas and Oregon. Under this project the capability to make bistatic observations has been developed and demonstrated whereby a radar at one site receives the transmissions of a radar from the other site, opening up a large set of potential propagation paths by which the condition of the ionosphere can be sensed. The separation of the sites exceeds 1000 km. Numerous 3-day bistatic campaigns were conducted over a period extending from September 2019 through March 2020. Three distinct bistatic propagation modes have been identified including a direct mode in which signals are transmitted and received through the radar side lobes. Direct mode signals propagate along the great-circle arc connecting the two bistatic radar sites, reflecting from the ionosphere at both E region and F region altitudes. Two additional modes are observed in which HF signals transmitted from one radar scatter from either ionospheric density irregularities or from the surface of the Earth before propagating to the bistatic receiving radar. Ray tracing simulations performed for examples of each mode show good agreement with observations and confirm our understanding of these three bistatic propagation modes [1]. The availability of a bistatic mode enables the radars to simulate a communications link and to help with the identification of propagation paths suitable for establishing links. AFRL personnel with related expertise and interest provided oversight and were consulted on the project.

2. INTRODUCTION

In this Section we provide the background for understanding the significance of making bistatic observations between pairs of Super Dual Auroral Radar Network (SuperDARN) HF radars.

The space environment of the Earth includes a layer of ionized gas extending from about 80 km altitude to the edge of deep space that is known as the ionosphere. Radio waves transit the ionosphere to establish communication links and to enable tracking with radar detection. The operation of Over-The-Horizon (OTH) radar systems depends on refraction in the ionosphere to bend radio waves to propagate along the limb of the Earth and so detect targets beyond the visible range limit. However, the ionosphere is highly variable, exhibiting orders of magnitude variations in density and spatial structure that are due to diurnal variation, solar variability, and geomagnetic activity. Knowledge of space environment conditions in the ionosphere is vital for understanding and mitigating the impacts of ionospheric variability on radio wave propagation.

SuperDARN is an international collaboration that operates low power, high-frequency (HF) scientific radars located in the midlatitude to polar regions of both hemispheres. The origins of

the network can be traced to the construction of a single radar located in Goose Bay, Labrador [2]. The network has expanded over the years to now consist of more than 35 radars of a similar design that are operated in a coordinated manner by scientists and funding agencies from ten different countries. SuperDARN radars are used individually and as a network in a variety of scientific experiments ranging from investigations of basic plasma phenomena to system-level science involving the large-scale plasma environment of Earth's ionosphere [3, 4]. Radars exist with many overlapping fields of view (FOVs) resulting in extensive coverage of the northern hemisphere above ~50° latitude in terms of AACGM coordinates [5]. Coverage is somewhat less extensive in the southern hemisphere where suitable land is less abundant.

The U.S. component of SuperDARN operates high frequency (HF) radars located at sites in Virginia (Blackstone and Wallops Island), Kansas (Fort Hays), and Oregon (Christmas Valley). The Fort Hays site is managed by a group at Virginia Tech (PI: J. Michael Ruohoniemi) and the Christmas Valley site by a group at Dartmouth College (PI: Simon G. Shepherd). Figure 1 shows an aerial view of the two radars that operate from the Christmas Valley site (CVW and CVE). Yellow lines highlight the antenna arrays of the eastward looking radar (CVE) that overlaps with the westward looking radar in Fort Hays (FHW). The inset in Figure 1 shows the rear antenna array of the CVE radar, with four antennas highlighted in cyan and corner reflector wires (used to improve directionality; front-to-back ratio) highlighted in green. The Twin-Terminated Folded Dipole (TTFD) antenna was specially developed for the U.S.-based SuperDARN radars [6].

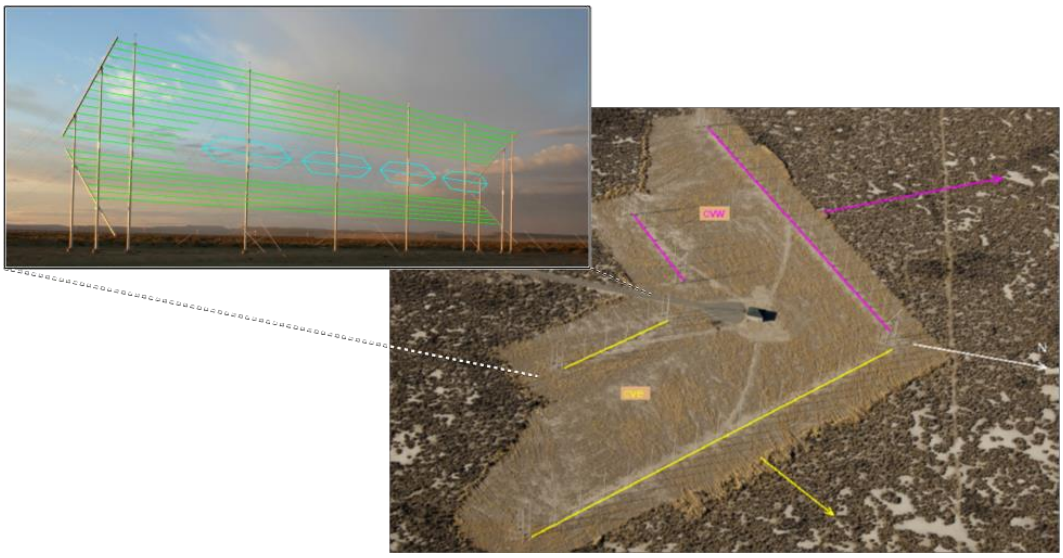

Figure 1. Aerial view of the SuperDARN radar facility near Christmas Valley, Oregon with close-up of antenna array

SuperDARN radars observe oblique backscatter from density irregularities in the ionosphere and function on the OTH radar principle in utilizing the properties of ionospheric refraction of HF radio waves to extend the radar fields of view to several thousand kilometers in range. Their primary scientific purpose has been to measure the velocity of ionospheric plasma as it is impressed on the irregularities and to study the connections of the ionosphere to the solar wind and to internal magnetospheric processes such as auroral substorms [7,8]. The measurements

also provide information on conditions within the ionosphere and on the availability of paths for HF surveillance and communications. Such ionospheric effects as multi-hop propagation, clutter, shortwave fadeout, and greyline propagation are routinely monitored with observations from the radars.

SuperDARN radars are phased array systems that operate on a continuous basis and typically scan over an azimuth extent of 50°-65° with a cadence of one minute. The operating frequency of individual radars can be varied over an 8–18 MHz range in order to achieve desirable propagation in the highly variable ionosphere. Figure 2 shows an example of simulating the propagation of HF radio waves along a particular beam direction of the FHW radar. Ray paths are numerically determined by "ray-tracing" in a model ionosphere; the International Reference Ionosphere (IRI) [9], color-coded by the electron density. The example shows rays paths (grey lines) refracting in the ionosphere near the density peak (red colors) and leading to somewhat complicated propagation paths. Of particular interest are the rays that achieve sufficient refraction as to become perpendicular to the magnetic field (pink lines extending through the figure approximately vertically) near the density peak. These locations are visible as black regions along the ray paths and indicate where ionospheric backscatter would occur if density irregularities were present. Measuring ionospheric backscatter over global scales is the primary objective of SuperDARN and forms the basis of many of the studies that use data from the network.

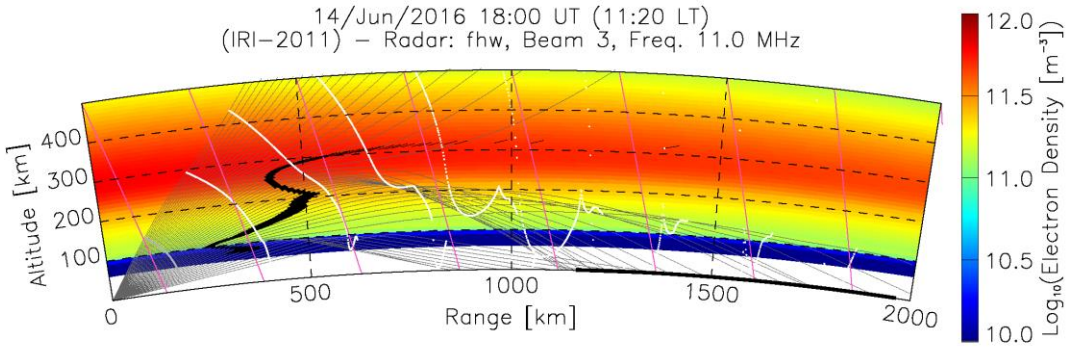

Figure 2. Numerical ray-tracing of radio waves through a model ionosphere along a particular beam of the Fort Hays radar

The other type of backscatter of interest for the proposed study is known as "ground scatter" or "sea scatter", whereby signals refract such that they return to the ground where they then reflect and follow the same path back to the transmitting radar. These types of rays can be seen in Figure 2 (marked with black on the Earth's surface where they reflect) and represent potential ground-to-ground HF communication links.

While there is significant coordination within the SuperDARN organization in the construction of radars and in operations and data sharing, the individual radars operate in a largely independent manner. Radars in the network collect data in common formats and follow a schedule of operation set by an internal SuperDARN committee, but each radar transmits and receives its own signal; that is, it operates in a monostatic fashion. In principle, it is possible for

SuperDARN radars to also receive signals from other radars in the network, that is, to operate in a bistatic or even multistatic manner. In doing so the radars would gain many more paths for making observations, for observing plasma irregularities with different wave numbers, and for providing additional information about the characteristics of the irregularities and their associated Doppler velocities, with the potential for greatly expanding the area for resolving directly the two-dimensional velocity vector.

The purpose of project was to demonstrate the capability to make bistatic observations directly with a pair of U.S. SuperDARN radars. In the course of this work protocols were developed to enable transmissions by the Fort Hays West radar (operated by Virginia Tech) to be received by the Christmas Valley East radar (operated by Dartmouth College), sites that are separated by a great circle distance of 1,819 km. This report is organized as follows: Section 3 describes various technical details of a bistatic operational mode for SuperDARN radars as well as experimental descriptions for numerous bistatic campaigns. Section 4 presents bistatic measurements from the two SuperDARN radars, highlighting three distinct modes of propagation. We report on the good agreement found between by comparing ray tracing simulations to the observations. In particular, we highlight the 'First Results' of bistatic observations [1]. We then summarize the results from this project and discuss the prospects of expanding the bistatic capability.

3. METHODS, ASSUMPTIONS, AND PROCEDURES

In this Section we describe how the radar operations were configured to support making bistatic observations. One significant technical detail was the need to synchronize transmission (Tx) and reception (Rx) across the radar sites to a high precision compared to the standard radar pulse width of 300 μs. In addition, we had to check that the radars colocated with the radars used for bistatic radars did not interfere with operations. These issues were resolved and the first confirmed bistatic observations were made on 8 January, 2019.

The two radar sites located near Christmas Valley, Oregon and Fort Hays, Kansas were chosen for the project. Constructed under the National Science Foundation (NSF) Mid-Sized Infrastructure (MSI) program in the years 2009-2011, these were the first two sites to host pairs of colocated SuperDARN radars and they share a common hardware and very similar operating software. The radars are labeled for their sites as FHW/FHE and CVW/CVE, where the trailing letter identifies the radar as oriented more eastward (E) or westward (W). The radars CVE and FHW were chosen for the project because they are oriented towards one another, resulting in large overlapping fields-of-view (FOVs). Figure 3 shows the geometry. The FOVs of the bistatic radars CVE and FHW are shown in light orange while the nonbistatic radar FOVs are shown in darker orange. Nominal beam directions for the bistatic radars are shown numbered in yellow. Sample beams are highlighted in magneta with a standard 45 km range resolution cells indicated. The dashed white line marks the bisector of the site locations, where ground points are equidistant from the two sites.

While it is possible to transmit and receive on both bistatic radars simultaneously, it would be difficult in that case to determine which radar was the source of any observation. In order to eliminate this ambiguity we chose to operate CVE in a receive-only manner while otherwise functioning normally but transmitting no power. The other bistatic radar (FHW in this case) operated normally; that is, it both transmitted and received its own signal while providing signal

for reception at CVE. The choice of CVE as the receive-only radar was made, in part, because this site has an operational interferometer array; a smaller four-element antenna array that is offset from the main 16-element array and is used to infer the elevation angle of the received signals [9]. For bistatic operations it was deemed more desirable to have elevation angle measurements at the receive end of the link to help resolve the propagation mode.

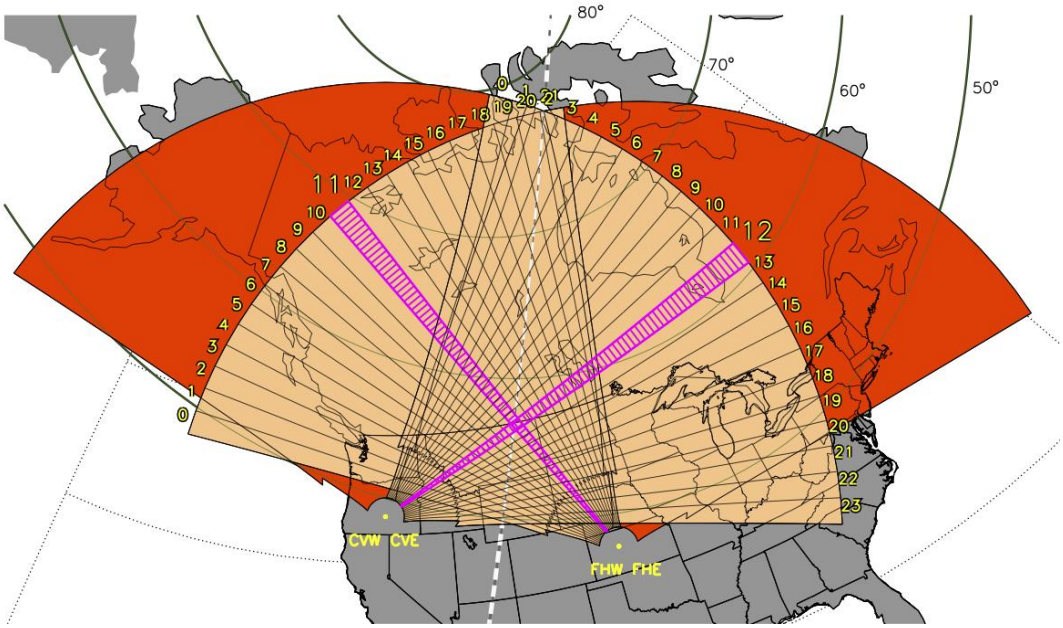

Figure 3. Fields of view of SuperDARN radars located at Christmas Valley, Oregon and Fort Hays, Kansas

An important technical detail necessary for making bistatic measurements is the synchronization of timing between the radars. To obtain range information from a distributed scattering region the SuperDARN radars utilize a multipulse transmission sequence that is analyzed to provide Doppler information (power, LOS velocity, and spectral width) over ranges often exceeding 4,000 km. A multipulse sequence typically consists of 9 – 11 pulses transmitted at varying time separations over a period of about 100 ms. Signal-to-noise ratio (SNR) is improved by integrating multiple sequences in a given beam direction. Typical integration periods are 3-7 s yielding 20-70 sequences. The transmission and reception of sequences must be synchronized across the radars in order to make sense of the bistatic measurements. For SuperDARN radars the range resolution along a beam direction is nominally determined by the length of individual pulses in the sequence and is typically 100-300 μs, corresponding to 15· to 45-km range resolution, respectively. Bistatic measurements require that the timing difference between the sites be limited to a small fraction of the pulse width, that is, <10 μs.

Network Time Protocol (NTP) is capable of maintaining time to within tens of milliseconds, which is not sufficiently accurate for our purposes. Instead, we use timing clocks in the radar computers that are synchronized using Global Positioning System (GPS) signals. Specifically, a GPS card installed in the computer that interfaces to the radar electronics at each site is used to generate regular timing pulses. The timing pulse initiates a sequence of timing signals that direct

the various hardware components to generate an transmit HF pulses and to receive and digitize incoming signals. We have found that GPS pulses generated at 7 Hz work well for bistatic operations.

Preliminary testing confirmed that the timing pulses from this GPS synchronization occur within ±5 μs of each other at the respective radar sites. The result is a better than 95% overlap of the transmission windows, even though one site is in receive-only mode. This level of synchronization is sufficiently accurate to support bistatic operations.

Before bistatic operation was first attempted, additional testing was performed at each radar site in order to eliminate the possibility of any coupling occurring between the collocated antenna arrays. For these tests the radar at each site that was not to be involved in the bistatic experiment (e.g., CVW and FHE) was set to operate monostatically (transmitting and receiving its own signal) while the second radar at the same site (e.g., CVE and FHW) was put into a bistatic mode where it simply received signals. It was confirmed that signals are indeed observed on the receive-only radars when the two collocated radars operate at identical frequencies. Coupling in this case maximizes when the main lobes of the collocated radars are pointed in the same direction, that is, along the bisector of the two array axes. Coupling occurs through radar side lobes and is greatly reduced when the radar main lobes are directed away from the common direction. For these reasons a frequency separation of ~50 kHz is imposed during all operations at the dual-radar sites, including during bistatic operations. When frequency separation is enforced, no significant coupling occurs between the radars.

Initial testing was conducted with the nonbistatic radars (CVW and FHE) remaining idle. However, during subsequent preliminary testing and bistatic campaigns these radars were operated in the standard manner (monostatic) in order to collect information about ionospheric propagation conditions and plasma flow over a larger region to provide contextual information for the bistatic observations.

After a limited amount of exploratory bistatic operation in which the operating frequency and beam combinations of the bistatic radars (CVE and FHW) were changed in a relatively ad hoc manner, a series of 3-day bistatic campaigns were implemented at the two sites. These campaigns were run during so-called discretionary time (DT) in the SuperDARN operating schedule. DT intervals, total 9 days each month, are scheduled around other experimental requests and typically occur on consecutive 3-day periods. During DT periods SuperDARN Principal Investigators (PIs) are free to perform maintenance on their radars, test experimental radar modes or operate their radars in any nonstandard manner they choose.

Beginning in September of 2019 the PI groups of the Oregon (CVW /CVE) and Kansas (FHW /FHE) sites scheduled their radars to operate in a bistatic manner during DT periods. For these campaigns a variety of experiments were performed in which the bistatic radars (CVE and FHW) operated on a preselected, common frequency (that could be varied in time) over a limited number of beam directions (ranging from 10 to 20). The nonbistatic radars (CVW and FHE) operated in the standard manner with the number of beam directions (or beams) during a radar scan (sampling of beams in a 1- to 2-min period) chosen to be commensurate with their bistatic

pair. All the radars at these sites operated with GPS time synchronization during the periods of bistatic operation.

Several different bistatic campaign scenarios were performed including operating at a single fixed frequency for a 24-hr period, transitioning between night (10.8 MHz) and day (13.8 MHz) frequencies and a frequency stepping arrangement whereby the bistatic radars operated for a 1-hr period at one of four set frequencies: 10.725, 11.8, 13.8 and 15.8 MHz. In most cases, the bistatic radars sampled 20 beams in a single 1-min scan corresponding to ~3 s integration per beam. The beams were chosen to be directed into the common-volume area of the two radars with a clockwise scanning sense for CVE (beams: 4-23) and counterclockwise for FHW (beams: 19-0).

Figure 3 shows two representative beams during the middle of a typical scan, with the two beams intersecting very near the radar site bisector line (dashed white trace). This symmetric beam pairing is the simplest to analyze since the paths between the radars and a common scattering point are then roughly the same. With the timing of the two radars synchronized for transmit and receive, CVE receives signals transmitted by FHW at the ranges that would be expected if it transmitted its own signal, assuming similar propagation and scattering conditions along the two paths. This mode has been used during most of the bistatic campaigns. The results shown in the next section were observed using this symmetric beam configuration, however, some campaigns have been conducted with nonsymmetric configurations. While the analysis is more difficult due to the differing propagation path lengths in this scenario, results from these campaigns are expected to reveal a more complete picture of the propagation and scattering conditions required to satisfy bistatic operations at HF. Analysis of bistatic observations with nonsymmetric beam configurations is left for future study.

4. RESULTS AND DISCUSSION

Over the course of the project bistatic operation was performed during discrete campaigns under a range of geomagnetic conditions. Table 1 summarizes the campaign times. A variety of bistatic modes were identified. In this Section we present in summary form examples of the three distinct modes of propagation that were most frequently observed during bistatic operation. Complete details for the examples summarized here are given in [1]. The modes are:

(1) direct transmission between the radar sites (direct mode)

(2) bistatic ground scatter (bistatic GS)

(3) bistatic ionospheric scatter (bistatic IS)

Figure 4 shows a schematic that illustrates the basic concept of these three bistatic modes. The direct mode is shown in red, bistatic GS in blue and bistatic IS in green. Solid lines of these colors represent raypaths that signals travel in the respective modes. Note that while bistatic signals travel from FHW to CVE for the majority of the bistatic campaigns, the reverse is also possible. Dashed, colored lines are projections of the raypaths onto the Earth. The site bisector is marked by a black, dashed line. For the direct mode there are two paths that follow the great-circle arc between the sites. These paths correspond to refraction back toward the ground occurring at E region and F region altitudes, respectively. There is no scattering involved in this

mode and despite separate paths we do not consider them separate modes because the basic mechanism is the same.

Table 1 . Bistatic Campaign Intervals

Start date	Start time (UT)	End date	End time (UT)
20190108	1900	20190108	1930
20190710	1653	20190710	1853
20190715	1946	20190715	2029
20190716	1800	20190717	1800
20190723	1800	20190724	1800
20190806	0100	20190806	1600
20190812	1930	20190812	1946
20190909	0000	20190911	2400
20190916	0130	20190918	2400
20190923	0230	20190925	2400
20191001	0000	20191003	2400
20191021	0100	20191023	2400
20191104	0100	20191106	2400
20191111	0000	20191113	2400
20191118	0130	20191122	2400
20191204	0000	20191206	1200
20191216	1500	20191218	2400
20200113	0000	20200115	2400
20200120	0000	20200122	2400
20200210	0000	20200212	2400
20200217	0300	20200219	2400
20200224	0000	20200226	2400
20200309	0000	20200310	2330
20200316	1600	20200318	2400
20200323	0000	20200325	2400
20200421	0000	20200421	2400
20200422	0000	20200422	2400
20200423	0000	20200423	2400
20200424	0000	20200426	2000
20200426	2000	20200426	2400
20200427	0000	20200427	2400
20200428	0000	20200429	2400

For the other two modes (bistatic GS and bistatic IS), refraction occurs but scattering is also required. For the bistatic GS mode signals are refracted back to the ground and scattering occurs from surface roughness. The scattering location for this mode is shown in Figure 2 by a solid blue circle. At this location some of the wave power is backscattered to the transmitting radar and some is scattered to the bistatic receiver. The mechanism for the bistatic IS mode is similar,

however, the scattering occurs from ionospheric plasma density irregularities, represented by black line-segments above the solid green circle in Figure 2, marking the scattering location for this mode.

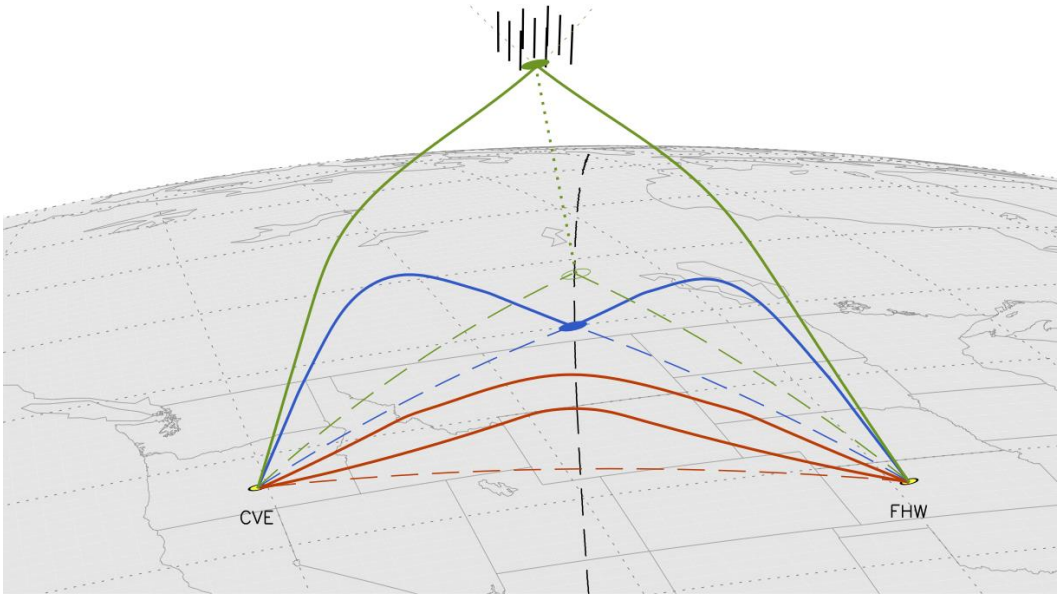

Figure 4. Schematic of three bistatic propagation modes

Many examples of these modes, often occurring simultaneously, were observed during the bistatic campaigns. Having selected representative examples of each mode, we show the observations and perform ray tracing simulations in order to confirm our understanding of the basic mechanisms for these bistatic modes of propagation.

Figure 5 shows observations from CVE and FHW over a 24-hr period during a campaign on 5 November 2019. The data shown are for beams 9, 11, and 13 of CVE and beam 12 of FHW (see beam numbers in Figure 1), from top to bottom. The color indicates the strength of the signal in dB above the sky noise. The vertical axis indicates the 45-km range gate number of the measurements with the upper limit corresponding to just below 2,500 km in range from the radar site. The signals observed by FHW (bottom panel) were collected in the usual Tx / Rx monostatic mode. However, all the signals observed by CVE originated from FHW and thus constitute bistatic signals. During this particular period the bistatic radars were stepped through a set of four frequencies (10.725, 11.8, 13.8 and 15.8 MHz) with the frequency remaining fixed for an hour at a time.

For the campaign shown in Figure 5 all three of the bistatic modes are observed. The direct mode can be seen during much of the 24-hr period and in all three panels of CVE data. It occurs in the narrow band of range gates from 18-20 corresponding to a range interval from ~990-1,080 km. The bistatic GS and IS modes are more intermittent and seen at farther ranges and over a wider range interval, ~1,080-1,980 km. In this example, the bistatic GS mode is observed primarily during daytime hours and has a wider range extent than the bistatic IS mode that is seen during

nighttime hours over a somewhat narrower range extent. All three modes exhibit significant variability with frequency, beam direction, and time of day. The bottom panel in Figure 5 shows monostatic backscatter along beam 12 of FHW occurs from meteors in the nearest ranges for the entire period, from ionospheric irregularities during nighttime hours, and from the ground during daytime hours. The observed overlap in monostatic backscatter and bistatic scatter is discussed further in the following subsection where the bistatic GS and IS modes are investigated in more detail.

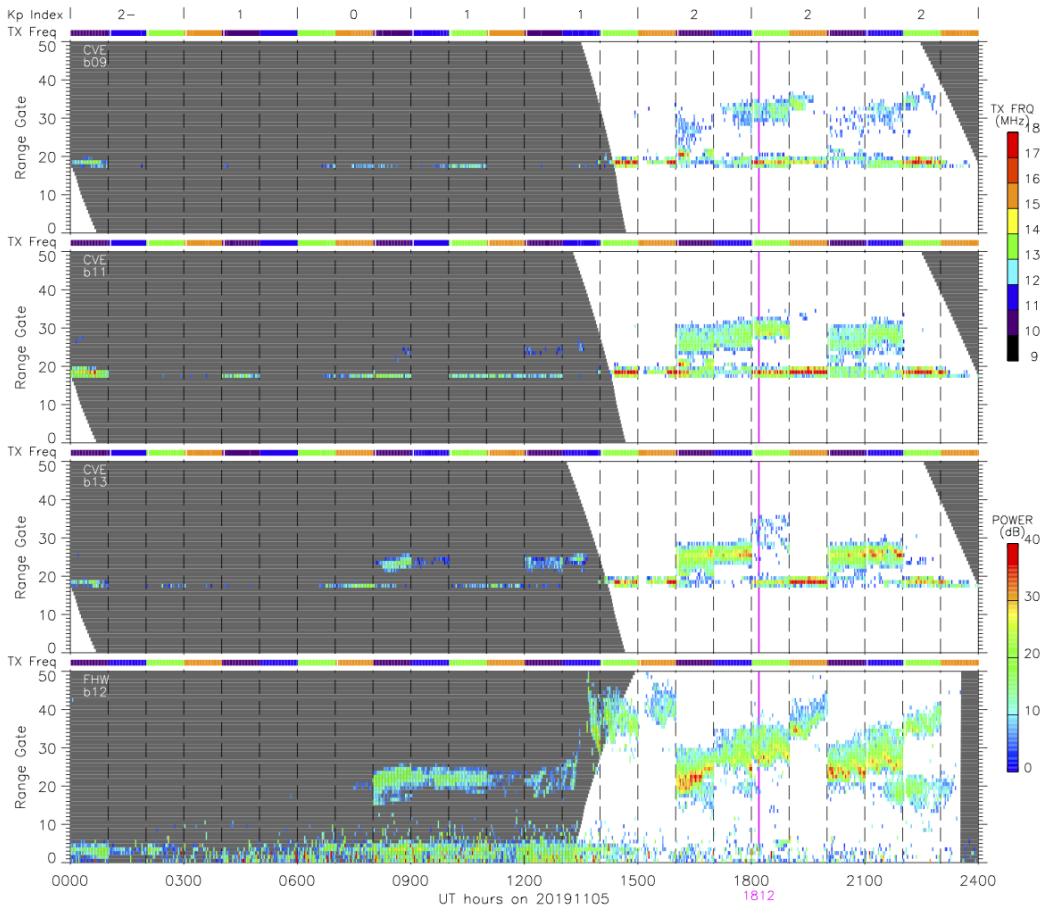

Figure 5. Stackplot of observations from beams of the CVE and FHW radars during bistatic operations on 5 November 2019

4.1. Direct Mode

The direct transmission mode is the name we give to signals that are transmitted from one radar (FHW) and propagate through the ionosphere directly to the receiving radar (CVE) following a great-circle arc. This mode is similar to that of an oblique sounder with one difference being that we are operating at a single frequency. It also simulates Tx /Rx operations between ground stations. This mode would presumably occur when the bistatic radars were operating with beams pointing directly at each. There is, however, no such beam combination (see Figure 1) and given that this mode is observed at a constant range over all of the beams in a 2-min scan, we surmise that the direct mode occurs through the radar side lobes.

Figure 6 shows a 2-min period of data from the Oregon (CVW/CVE) and Kansas (FHW /FHE) radars from 18:12-18:14 UT on 5 November 2019 (indicated by the vertical magenta line in Figure 3). The bistatic radars (CVE and FHW) were operating at 13.8 MHz during this period, while CVW was operating at 14.7-15.0 MHz and FHE was operating at 11.4-11.6 MHz. The observed Doppler LOS velocity (vws) is shown according to the blue-red color scale. Low-velocity magnitude (<10 m s^{-1}) is indicated with light gray for nonbistatic radars (CVW and FHE), darker gray for FHW and green for CVE. Furthermore, the bistatic observations from CVE are highlighted in yellow outline for clarity.

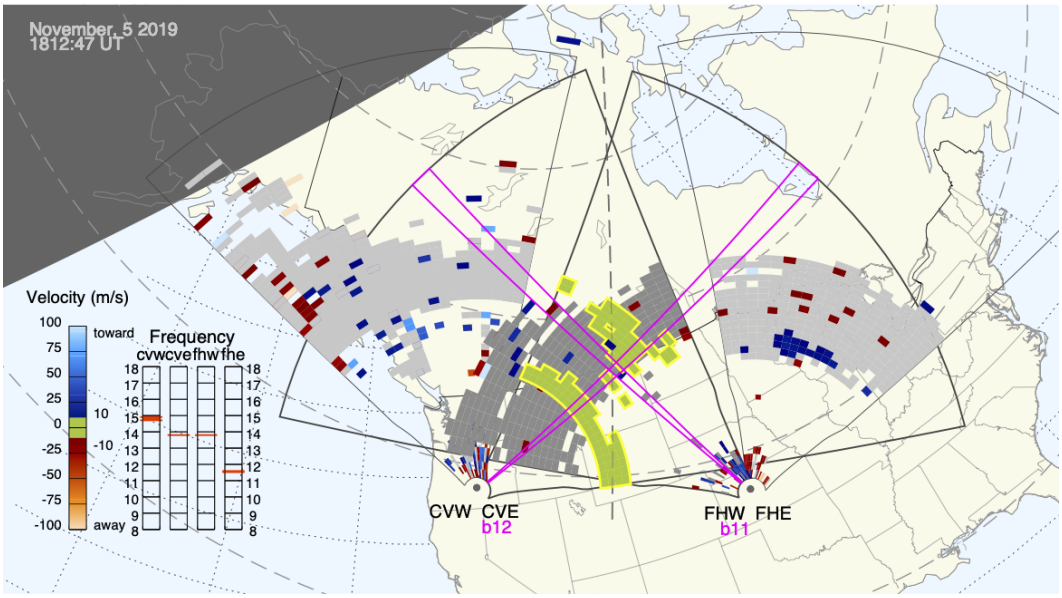

Figure 6. Radar observations for a 2-min period from 18:12 – 18:14 UT on 5 November 2019 during a bistatic campaign

During this period the nonbistatic radars and FHW were observing bands of ground or sea backscatter that extended over the entire azimuthal extent of the radar FOVs. Ground scatter, as it is commonly referred to, occurs when signals transmitted by a radar refract sufficiently in the ionosphere so that they propagate back to the ground (or sea) at some distance from the radar. There, the signals encounter roughness and some power is scattered back to the radar. The so-called skip distance is the distance on the Earth's surface that the signals travel between the radar and the point where they are reflected from the ground. Because the skip distance depends on the radar frequency and the density of the ionosphere, ground scatter can be used to determine ionospheric conditions in the radar FOV. In addition, ground scatter often reveals details of atmospheric gravity wave activity associated with traveling ionospheric disturbances as the observed skip distance is modulated by changes in the ionospheric density.

The direct mode, as seen in Figure 6, occurs over a constant range interval (three range gates in this example) over the entire scan of CVE radar beams. Here we are using the standard SuperDARN analysis software, commonly referred to as the Radar Software Toolkit (RST) [11],

which is designed for monostatic operation and, therefore, maps the position of signals based on the assumption of round-trip propagation. For this reason, the direct mode observations appear at a distance that is half of the actual travel distance, that is, at the halfway point along the great-circle arc between the bistatic radars.

The direct mode appears at a constant range because the propagation path between the radars is relatively constant through the side lobes while the software assumes the observations are in the direction of the main lobe. The result is the arc, colored green for low velocity, appearing in range gates 18-20. Variations in the signal strength with time and beam direction can be attributed to operational factors, such as the relative side lobe strength of a particular beam combination, and the operating frequency. Note that side lobes can be as high as -10 dB in certain situations [5]. In addition, some of the variation is clearly geophysical in nature as the ionospheric density changes along the propagation path due to external influences, the most obvious being the very strong signals observed during the daytime at the higher frequencies when the ionospheric densities are largest.

In order to understand the details of signals propagating between the radars in the direct mode, we performed ray tracing simulations of the HF signal in a model ionosphere given by the latest version of the International Reference Ionosphere (IRI-2016). The ray tracing code is a modified version from that presented in [12], which uses an adaptive step size Runga-Kutta solver to determine the raypaths of HF waves in an unmagnetized plasma.

Figure 7 shows the results of the ray tracing simulations for the conditions given by the IRl-2016 model and the operational radar parameters used at 18:12-18:14 UT on 5 November 2019. The background color indicates the electron density given by the IRl-2016 model along the great-circle path between the two bistatic radars. Two representative electron density profiles, on a logarithmic scale, are shown at 0- and 1,819-km ground range. Projections of the magnetic field from the International Geomagnetic Reference Field (IGRF) are indicated with pink lines spaced at 500-km intervals at 400-km altitude.

In this simulation a set of rays consisting of electromagnetic waves at 13.8 MHz are launched from the location of CVE with elevation angles ranging from 0° to 35°. The decision to have the rays originate from CVE was chosen for simplicity in determining elevation angles. Reciprocity is assumed and the elevation angles on receive are therefore the same as the launch angles, which are specified for each ray. The paths of representative rays are shown in gray, with darker gray used to indicate penetrating rays, that is, rays that do not return to the surface of the Earth. Rays that return to the ground within ±45 km (one range gate) of the location of FHW are highlighted in magenta. These rays represent potential paths for signals to travel directly between the two radars. Note that the vertical scale in Figure 7 is doubled in order to emphasize the region of interest in the ionosphere while showing the entire raypath; as a consequence, some ray paths may appear distorted.

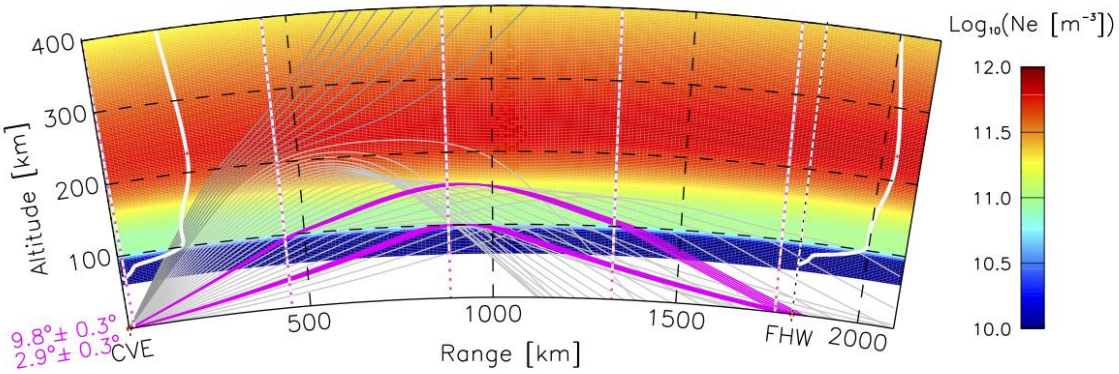

Figure 7. Ray tracing simulation of the direct mode at 18:12 UT on 5 November 2019

It is evident from these simulations that two possible paths exist for the direct mode: one that refracts back toward the ground in the E region and another that does the same at a higher altitude in the F region. Rays traveling along the longer F region path would appear at ranges further from the radar than those traveling along the shorter E region path. If both paths exist at a given time, one might therefore expect observations of the direct mode at multiple ranges. This is explained by the direct mode being observed over three range gates during the daytime. An example of two simultaneous, yet separated in range, observations of the direct mode was captured when a bistatic campaign was operated with 15-km range resolution (not shown). With the higher resolution two distinct bands were observed that corresponded to the E region and F region paths predicted by the ray tracing simulations.

4.2. Bistatic Ground Scatter Mode

The other bistatic mode observed at 18:12 UT in Figures 5 and 6 is the bistatic GS mode. This mode is similar to ground backscatter observed during monostatic operation; however, the signal observed by the bistatic receiver originates from the bistatic transmitter and is scattered from the location on the ground where the rays are reflected in the direction of the bistatic receiving radar. Figure 6 (and to some extent Figure 5) reveals that the bistatic GS mode is observed where the bistatic beams overlap in an area where ground backscatter is observed by the transmitting radar operating in monostatic mode, that is, FHW.

During the period shown in Figure 6, the bistatic radars were operating with symmetric beam pairings and the beams, therefore, intersect along the bisector of the two radar sites. The overlapping region in this case occurs where the radar bisector intersects the ground backscatter band observed by the transmitting radar. In this situation the paths to the scattering point are similar and bistatic observations are only possible where ground backscatter is also occurring along the transmission leg. The location of the bistatic GS observations will, therefore, move as the location of the ground backscatter (skip distance) responds to changes in the density of the ionosphere and the operating frequency.

It can be seen in Figure 6 that radars are operating at different frequencies and as a consequence both the skip distance of their respective ground backscatter bands, and the extent of the bands, differ. In this case the skip distance is proportional to the operating frequency, whereas the range extent varies inversely with frequency. Ground backscatter appears closest to the FHW radar that is operating at the lowest frequency (~11.5 MHz) during this time and the extent of the band is the greatest. Note that some deviation from this expected behavior is observed in the zonal directed beams of CVW and FHW. These beams sample parts of the ionosphere that are very different from those sampled by the poleward directed beams, which illustrate the expected dependence.

Figure 5 shows that bistatic GS observations (top three panels) track variations in the transmitting radar skip distance (bottom panel) as the frequency changes at hour intervals. In the daytime hours the band of bistatic GS observations narrows in extent and increases in range as the frequency increases, as expected.

As with the direct mode, we perform a ray tracing simulation using the ionospheric density specified by the IRI-2016 model during the time when the bistatic GS mode was observed. Unlike the monostatic or direct mode situation rays in the bistatic GS mode propagate along two separate paths through the ionosphere. We perform the ray tracing along separate two-dimensional planes in the directions of the bistatic radar beams. In this case we propagate rays originating from both bistatic radar sites (CVE and FHW) and look for those rays that return to the ground within one 45-km range gate of the beam intersection location.

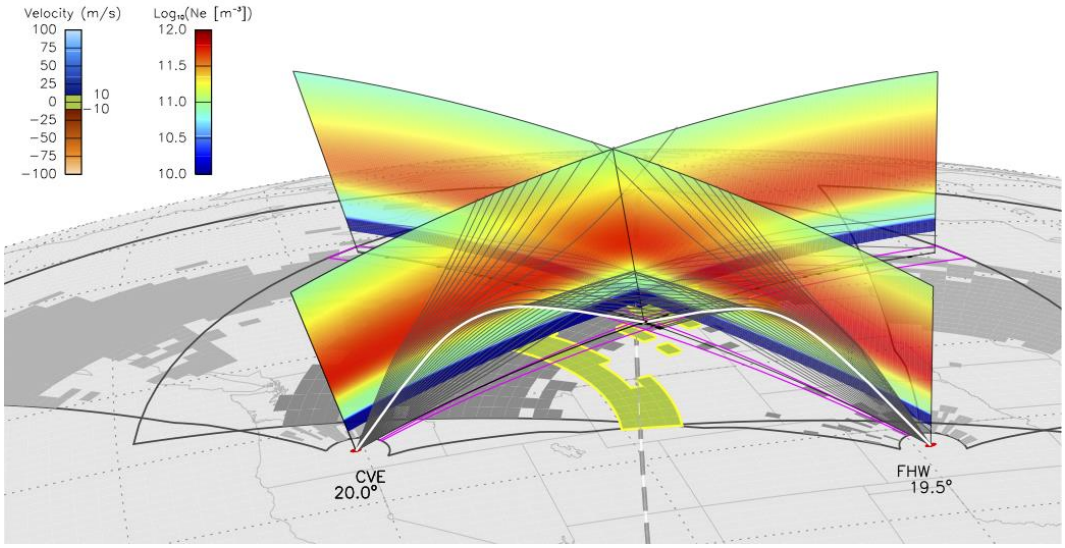

Figure 8. SuperDARN observations and ray tracing simulations at 18:12 UT on 5 November 2019

Figure 8 shows the results of the ray tracing simulation for the 1-min period starting at 18:12 UT on 5 November 2019. Measurements from the four radars are shown on the map. The ionospheric density obtained from the IRI-2016 model is shown along two representative beam directions (CVE: 12, FHW: 11). Rays with elevation angles in the range 0 °-35° are shown in gray. Some of these rays penetrate the ionosphere and others return to the ground at a distance

from the radars. The rays that return to the ground within the beam intersection region are highlighted in white. Collectively, these are the possible paths for bistatic signals to propagate from FHW to CVE in the bistatic GS mode. Simulations along the other beam combinations occurring during this period indicate that a viable path for the bistatic GS mode exists in the region where the beam intersection overlaps the ground backscatter band from the transmitting radar.

One other measurable we are able to compare with the output of the simulations is the elevation angle. Figure 7 shows that the elevation angles at CVE satisfying the criteria for the bistatic GS mode during this period were within a degree of 20°. This value was the maximum obtained from simulations of the other beam combinations, which also showed the elevation angle decreasing as the intersection point moves further from the radars. Analysis of elevation angle measurements from CVE shows a well-defined and narrow peak (~3° wide), likely due to the localization of these bistatic measurements along the radar bisector, at ~22.5°. The agreement between the observed elevation angles and those obtained from the ray tracing simulation are generally good, supporting the idea that the observations are indeed propagating in the bistatic GS mode.

4.3. Bistatic Ionospheric Scatter Mode

The third propagation mode observed during our campaigns we refer to as bistatic IS. In this case signals transmitted from FHW scatter from ionospheric irregularities at F region altitudes and return to the bistatic receiver at CVE, in addition to returning to the transmitting radar. In this scenario, as with the monostatic situation, the Doppler velocity of the received signals is a measure of a component of the E x B plasma drift.

While the bistatic IS mode was observed on 5 November 2019 (Figure 5) during nighttime hours, we choose an example from another period on 1 October 2019 to investigate this mode in more detail. Figure 9 shows observations for the 24-hr period on this day from a single beam of all four SuperDARN radars located in Oregon and Kansas. From top to bottom, the selected beams are CVW beam 18, CVE beam 13, FHW beam 10, and FHE beam 5. Overall geomagnetic activity is somewhat elevated during this period as indicated by Kp values ranging from 2+ to 4 during the first 12 hours. Relatively strong and highly variable flows exceeding 100 m/s can be seen in the nonbistatic radars (CVW and FHE) for the early part of the period, up to ~08:00 UT. The sense of flow during this period is in the westward direction as indicated by the red/blue colors of west/easterly directed beams of the CVW /FHE radars shown in the top/bottom panels of Figure 9.

The interval of interest on this day begins near 01:30 UT and continues for approximately 30 min. During this time the bistatic radars were operating at 11.8 MHz. FHW observes a relatively narrow but expanding patch of backscatter flowing in the westward direction. At the same time CVE observes a narrow patch of bistatic scatter with low velocities. The CVE measurements during this interval are thought to be propagat-ing in the bistatic IS mode. We have selected the period at 01:44 UT, marked by the vertical magenta line in all panels of Figure 9, to investigate this mode in more detail. Note that during the daytime hours both the direct mode and bistatic GS mode are also observed by CVE on this day.

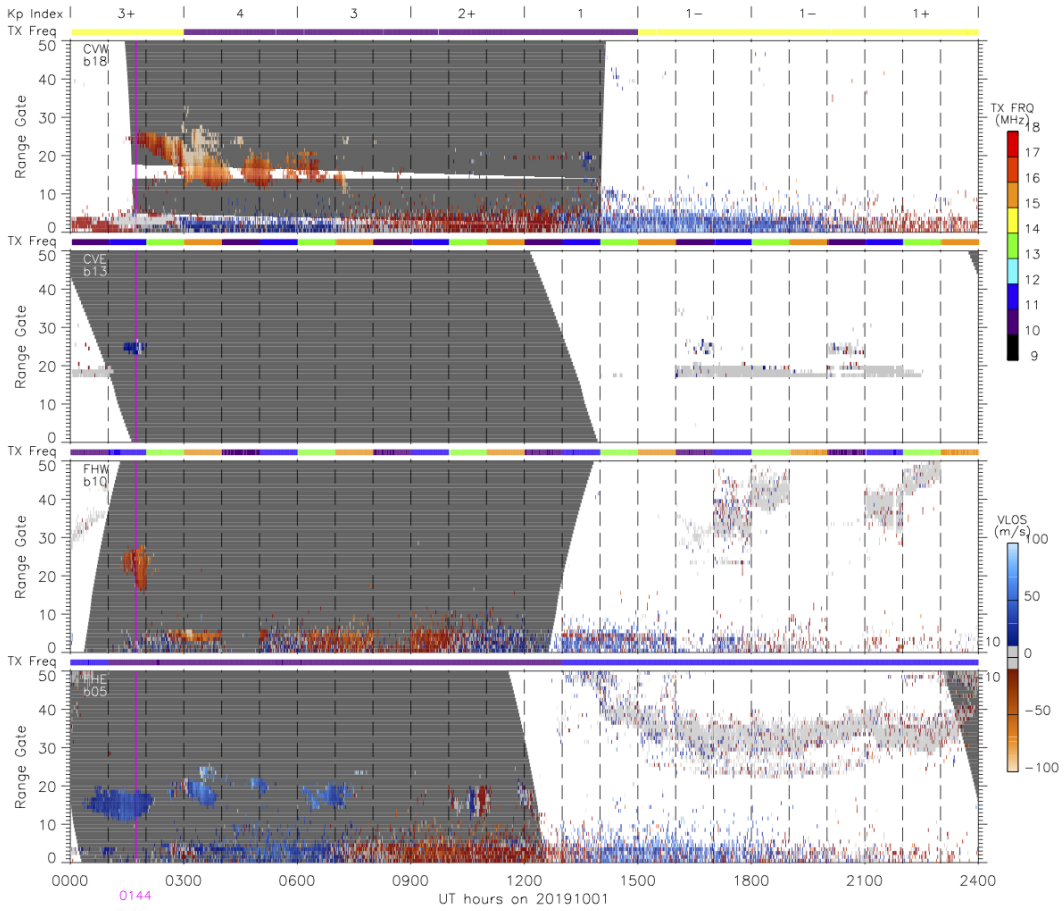

Figure 9. Stackplot of observations on 1 October 2019 from one beam of each SuperDARN radar in Oregon and Kansas

Figure 10 shows measurements from all four SuperDARN radars during the 1-min scan period beginning at 01:44 UT on 1 October 2019 in which each radar samples 20 beam directions for 3 s each. The main backscat-ter feature during this time is the relatively narrow (<10° AACGM latitude) channel of westward directed flow seen by the three radars operating monostatically (CVW, FHW and FHE). The sense of the LOS flow alternates between toward and away across the three radars as the dominant sense of azimuthal direction of radar FOY alternates. The gray color seen in the FHW FOV indicates where the flow direction is perpendicular to the radar beam direction, and hence, Vlos is close to zero. Analysis of the azimuthal dependence of Vlos for this period indicates that the measurements are consistent with westward directed flow that is increasing in magnitude the further west the flow is measured, suggesting that the radars are observing a relatively low-velocity subauroral polarization stream (SAPS).

The signal observed by the bistatic receiver at CVE is highlighted in yellow in Figure 10. The extent of these measurements is limited, but as was the case with the bi static GS mode, the measurements occur where the CVE beam overlaps the monostatic observations from FHW that reveal the relatively narrow SAPS channel. In this case the observations occur along the radar site bisector due to the symmetric beam sampling that was used during this period. These signals, which propagate in the bistatic IS mode, are transmitted from FHW and refract in the ionosphere

before scattering from ionospheric density irregularities. The signal that returns to FHW is the standard ionospheric backscatter observed during monostatic operations, while the signal observed by CVE has been scattered by irregularities in the direction of the bistatic receiver. In addi-tion, the bistatic geometry requires the presence of ionospheric irregularities with a larger scale size than those needed in the monostatic case. For the beam combinations with which the bistatic IS mode is observed during this period, the scattering irregularities are a factor of ~1.30-1.45 larger in scale length than those responsible for the observed monostatic ionospheric backscatter.

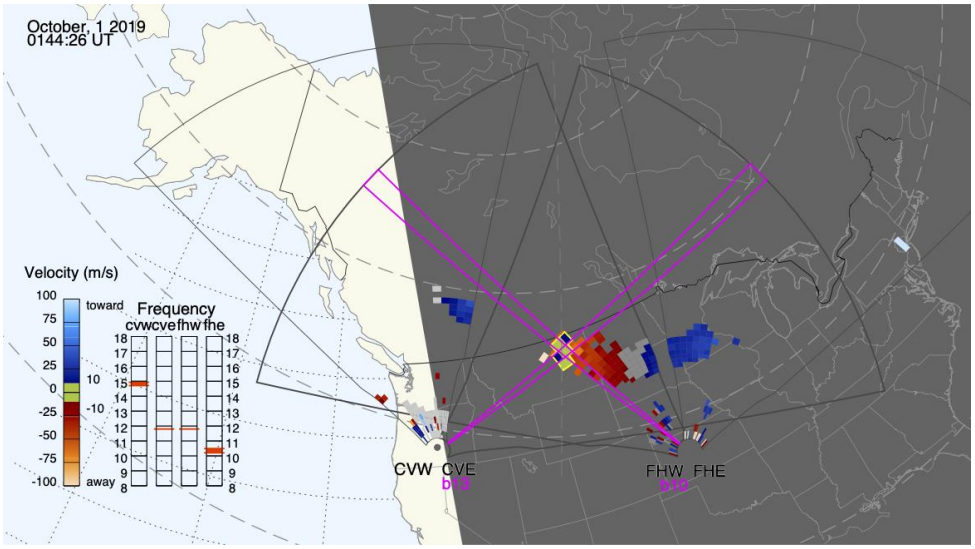

Figure 10. SuperDARN observations for a 1-min period beginning at 01:44 UT on 1 October 2019 during a bistatic campaign

The basic concept of the bistatic GS mode and the bistatic IS mode is the same; signals are transmitted from the one radar, refract in the ionosphere, and are then scattered in the direction of the second, receive-only radar. The difference is in the scattering mechanism. For the bistatic GS mode signals are scattered from the ground or sea whereas irregularities in the ionosphere are the source of scattering for the bistatic IS mode. Unlike the bistatic GS example, no direct mode was observed during this time.

We perform a similar ray tracing simulation with the bistatic IS mode observations in order to confirm that this mode was viable during this period. Figure 11 shows the ray tracing results for the 1-min period beginning at 01:44 UT on 1 October 2019. As with the simulation of the bistatic GS mode, radar measurements during this time are shown on the map. The electron density obtained from the IRI-2016 model for this per-iod is shown along the same beam directions displayed in Figure 7. Of particular note is the lower electron density for this period, as would be expected during the nighttime when solar ionization is absent and recombination reduces the ionospheric density. One addition to Figure 11 is the short black line-segments, which indicate the location along individual ray paths where the wave k-vector is perpendicular to the local magnetic field (indicated by vertical pink lines). These locations show where conditions exist for the signal to be backscattered to the transmitting radar. In the case of monostatic operation these

mark the locations where radar backscatter would be expected in the presence of suitable irregularities. In fact, FHW observed backscatter that is consistent with this geometry.

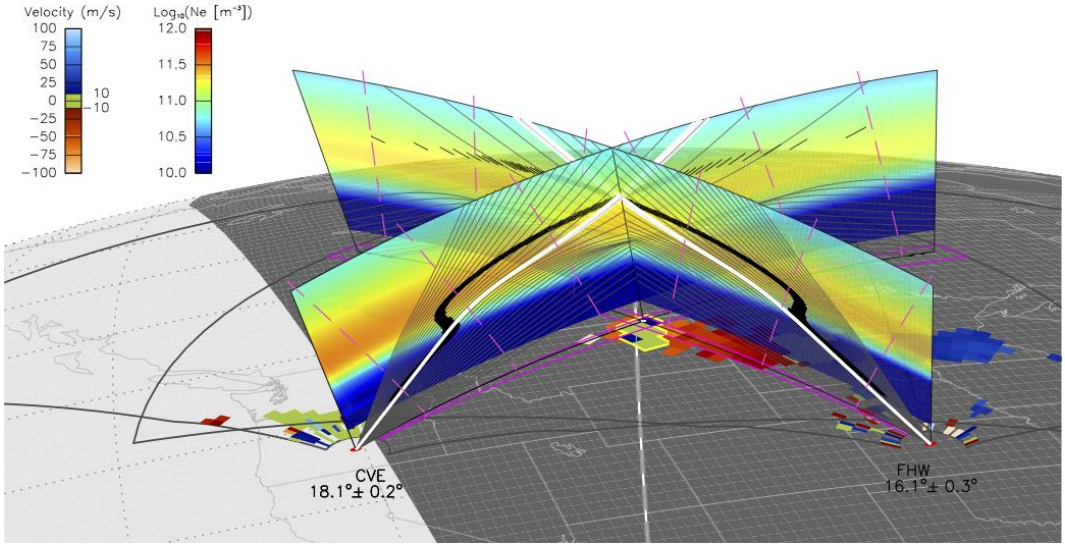

Figure 11. SuperDARN observations and ray tracing simulations for 01:44 UT on 1 October 2019

While a full three-dimensional analysis of the scatter region and resulting propagation along the reception path is required for bistatic operations, we again choose to demonstrate the viability of this mode by perform-ing ray tracing from CVE to the potential scattering region and assuming that reciprocity holds. We highlight by performing ray tracing from CVE to the potential scattering region and assuming that reciprocity holds. We highlight the rays in white that satisfy the conditions for signals propagating in the bistatic IS mode, that is, the rays that are within 1° of perpendicularity to the local magnetic field in the region where the bistatic radar beams intersect. These are the rays for which the bistatic IS mode is a viable propagation path for bistatic observations during this time.

5. CONCLUSIONS

This report describes the progress of a cooperative project involving Virginia Tech, Dartmouth College, and AFRL to perform the first bistatic operations between SuperDARN HF radars. This technical goal was realized and additional analysis was performed to aid in the interpretation of the observations and to advance scientific understanding. The first results were reported in [1]. In this Section we summarize the work performed and the conclusions reached.

Super DARN radars operate primarily in a monostatic configuration in which HF signals transmitted from a radar propagate in the ionosphere and backscatter from ionospheric density irregularities at E region or F region altitudes, or from the Earth's surface, before returning to the same radar. These radars cover a large portion of the Earth's polar regions and measurements

from the network are used in numerous studies of the thermosphere-ionosphere-magnetosphere system [3,4].

We have developed the necessary hardware and software to operate, for the first time, SuperDARN HF radars in a bistatic manner whereby HF signals transmitted from one radar are received and analyzed by another radar that is separated by a distance > 1,000 km. Initial testing with radars located in Oregon and Kansas confirms that sufficient timing accuracy is achieved for bistatic operation by using GPS synchronized clocks. Furthermore, the imposed frequency separation with the colocated second radar at these dual-radar sites prevents any unwanted signals due to coupling.

A series of 3-day bistatic campaigns were performed over a period from September 2019 to March 2020 in which the CVE radar in Oregon was operating bistatically with the FHW radar located in Kansas. During these campaigns signals transmitted by FHW were received and analyzed by the CVE radar. The nonbistatic radars, CVW and FHE, and the FHW radar, received and analyzed their own signals, providing contextual information about the ionosphere in the nearby region.

1. Direct mode-HF signals are transmitted from FHW and received by CVE through radar side lobes in the vertical plane defined by the great-circle arc along the Earth's surface that joins the sites. Refraction from both E region and F region altitudes can occur independently or simultaneously, depending on the ionospheric densities along the propagation path between the bistatic radars. This mode is observed over a fixed range interval, often in all beam directions but with varying amplitude, and is more commonly seen during the daytime when ionospheric densities are largest.
2. Bistatic ground scatter mode-HF signals propagate from the transmitting radar (FHW) into the ionosphere and refract back toward the Earth where they are scattered from the surface. For monostatic radars the scattered signal propagates back to the transmitting radar along the same path. For the bistatic GS mode the scattered signal propagates along a similar path in the direction of the bistatic receiver, CVE in this case. Bistatic GS mode scatter is observed where the two radar beams overlap and ground back-scatter is observed by the transmitting radar in its monostatic configuration. For the case where the beams are scanned symmetrically, the intersection point occurs along the radar site bisector.
3. Bistatic ionospheric scatter mode-HF signals propagate in a similar manner to the bistatic GS mode, however, scattering occurs from ionospheric density irregularities. Backscatter is received on the mono-static transmitter and the observed Doppler V_{los} is a component of the EXB drift velocity (assuming the backscatter occurs at F region altitudes). Scatter received by the bistatic radar propagates in the bistatic IS mode and the observed Doppler V_{los} is in the direction that bisects the transmission and reception beams. As with the bistatic GS mode, bistatic IS mode observations occur where radar beams intersect and backscatter is observed by the transmitting radar.

In order to explain the various modes of propagation that were observed during bistatic operation, we performed ray tracing simulations for examples of each of the three modes. The simulations were performed using electron densities specified by the IRI-2016 model in the

vertical planes appropriate to the various propagation modes. In all cases electron densities were unmodified from the values obtained by the IRI-2016 model and the agreement between the predicted and observed propagation paths of bistatic scatter observations varied but was generally reasonable.

REFERENCES

[1] Shepherd, S. G., Sterne, K. T., Thomas, E. G., Ruohoniemi, J. M., Baker, J. B. H., Parris, R. T., et al. (2020), Bistatic observations with SuperDARN HF radars: First results. *Radio Science*, **55**, e2020RS007121, https://doi.org/10.1029/2020RS007121.

[2] Greenwald, R. A., Balcer, K. B., Dudeney, J. R., Pinnock, M., Jones, T. B., Thomas, E. C., et al. (1995), DARN/Super DARN: A global view of the dynamics of high-latitude convection, *Space Science Reviews*, **71**, 761, https://doi.org/10.1029/95JA01215.

[3] Chisham, G., Lester, M., Milan, S.E., Freeman, M.P., Bristow, W.A., Grocott, A., MacWilliams, K.A., Ruohoniemi, J. M., Yeoman, T.K., Dyson, Greenwald, P R.A., Kikuchi, T., Pinnock, M., Rash, J., Sato, N., Sofko, G., Villain, J.-P, and Walker, A.D.M., A decade of the Super Dual Auroral Radar Network (SuperDARN): Scientific achievements, new techniques and future directions, *Surveys in Geophysics*, **28**, pp. 33-109, doi:10.1007/s10712-007-9017-8, 2007.

[4] Nishitani, N., Ruohoniemi, J.M., Lester, M., Baker, J.B.H., Koustov, A.V., Shepherd, S.G., Chisham, G., Hori, T., Thomas, E.G., Makarevich, R.A., Marchaudon, A., Ponomarenko, P., Wild, J., Milan, S.E., Bristow, W.A., Devlin, J., Miller, E., Greenwald, R.A., Ogawa, T., and Kikuchi T., (2019), Review of the accomplishments of Mid-latitude Super Dual Auroral Radar Network (SuperDARN) HF Radars, *Progress in Earth and Planetary Science*, **6:27**, https://doi.org/10.1186/s40645-019-0270-5.

[5] Shepherd, S. G. (2014), Altitude-adjusted corrected geomagnetic coordinates: Definition and functional approximations, *J. Geophys. Res.,* **119**, doi: 10.1002/2014JA020264.

[6] Sterne, K.T., Greenwald, R.A., Baker, J.B.H., and Ruohoniemi, J.M., Modeling of a twin terminated folded dipole array for the Super Dual Auroral Radar Network (SuperDARN), *Proceedings of the 2011 IEEE Radar Conference*, IEEE, ISBN 978-1-4244-8902-2, pp 934-938, 23-27 May 2011.

[7] Ruohoniemi, J. M. and Baker, K. B., Large-scale imaging of high-latitude convection with SuperDARN HF radar observations, *J. Geophys. Res*., **103**, pp. 20797-20811, 1998.

[8] Shepherd, S. G. and Ruohoniemi, J. M., Electrostatic potential patterns in the high latitude ionosphere constrained by SuperDARN measurements, *J. Geophys. Res.*, **105**, 23005-23014, 2000.

[9] Bilitza, D., Altadill, D.,Truhlik, V.,Shubin,V.,Galkin, I., Reinisch, B., and Huang,X. (2017), International Reference Ionosphere:2016 From ionospheric climate to real-time weather predictions. *Space Weather,***15***, pp.* 418-429, https://doi.org/10.1002/2016SW001593.

[10] Shepherd, S. G. (2017), Elevation angle determination for SuperDARN HF radar layouts, *Radio Science*, **52**, pp. 938-950, https://doi.org/ IO.I002/2017RS006348.

[11] Thomas, E.G.,Sterne, K.T.,Shepherd, S. G., Kotyk, K.,Schmidt, M., Ponomarenko, P.V., et al. (2019), SuperDARN RadarSoftwareToolkit (RST) 4.3, https://doi.org/10.5281/:zenodo.3401622.

[12] de I.arquier, S., Ponomarenko, P., Ribeiro, A. J., Ruohoniemi, J. M., Balcer, J. B. H., Sterne,K.T., and Lester, M. (2013), On the spatial distributionof decarneter-scale subauroral ionospheric irregularities observed by SuperDARN radars. *J. Geophys. Res.*, **118**, pp. 5244-5254, https://doi.org/10.1002/jgra.50475.

REFERENCES

[1] Shepherd, S. G., Sterne, K. T., Thomas, E. G., Ruohoniemi, J. M., Baker, J. B. H., Parris, R. T., et al. (2020), Bistatic observations with SuperDARN HF radars: First results. *Radio Science*, **55**, e2020RS007121, https://doi.org/10.1029/2020RS007121.

[2] Greenwald, R. A., Balcer, K. B., Dudeney, J. R., Pinnock, M., Jones, T. B., Thomas, E. C., et al. (1995), DARN/Super DARN: A global view of the dynamics of high-latitude convection, *Space Science Reviews*, **71**, 761, https://doi.org/10.1029/95JA01215.

[3] Chisham, G., Lester, M., Milan, S.E., Freeman, M.P., Bristow, W.A., Grocott, A., MacWilliams, K.A., Ruohoniemi, J. M., Yeoman, T.K., Dyson, Greenwald, P R.A., Kikuchi, T., Pinnock, M., Rash, J., Sato, N., Sofko, G., Villain, J.-P, and Walker, A.D.M., A decade of the Super Dual Auroral Radar Network (SuperDARN): Scientific achievements, new techniques and future directions, *Surveys in Geophysics*, **28**, pp. 33-109, doi:10.1007/s10712-007-9017-8, 2007.

[4] Nishitani, N., Ruohoniemi, J.M., Lester, M., Baker, J.B.H., Koustov, A.V., Shepherd, S.G., Chisham, G., Hori, T., Thomas, E.G., Makarevich, R.A., Marchaudon, A., Ponomarenko, P., Wild, J., Milan, S.E., Bristow, W.A., Devlin, J., Miller, E., Greenwald, R.A., Ogawa, T., and Kikuchi T., (2019), Review of the accomplishments of Mid-latitude Super Dual Auroral Radar Network (SuperDARN) HF Radars, *Progress in Earth and Planetary Science*, **6:27**, https://doi.org/10.1186/s40645-019-0270-5.

[5] Shepherd, S. G. (2014), Altitude-adjusted corrected geomagnetic coordinates: Definition and functional approximations, *J. Geophys. Res.,* **119**, doi: 10.1002/2014JA020264.

[6] Sterne, K.T., Greenwald, R.A., Baker, J.B.H., and Ruohoniemi, J.M., Modeling of a twin terminated folded dipole array for the Super Dual Auroral Radar Network (SuperDARN), *Proceedings of the 2011 IEEE Radar Conference*, IEEE, ISBN 978-1-4244-8902-2, pp 934-938, 23-27 May 2011.

[7] Ruohoniemi, J. M. and Baker, K. B., Large-scale imaging of high-latitude convection with SuperDARN HF radar observations, *J. Geophys. Res*., **103**, pp. 20797-20811, 1998.

[8] Shepherd, S. G. and Ruohoniemi, J. M., Electrostatic potential patterns in the high latitude ionosphere constrained by SuperDARN measurements, *J. Geophys. Res.*, **105**, 23005-23014, 2000.

[9] Bilitza, D., Altadill, D.,Truhlik, V.,Shubin,V.,Galkin, I., Reinisch, B., and Huang,X. (2017), International Reference Ionosphere:2016 From ionospheric climate to real-time weather predictions. *Space Weather,***15***, pp.* 418-429, https://doi.org/10.1002/2016SW001593.

[10] Shepherd, S. G. (2017), Elevation angle determination for SuperDARN HF radar layouts, *Radio Science*, **52**, pp. 938-950, https://doi.org/ IO.I002/2017RS006348.

[11] Thomas, E.G.,Sterne, K.T.,Shepherd, S. G., Kotyk, K.,Schmidt, M., Ponomarenko, P.V., et al. (2019), SuperDARN RadarSoftwareToolkit (RST) 4.3, https://doi.org/10.5281/:zenodo.3401622.

[12] de I.arquier, S., Ponomarenko, P., Ribeiro, A. J., Ruohoniemi, J. M., Balcer, J. B. H., Sterne,K.T., and Lester, M. (2013), On the spatial distributionof decarneter-scale subauroral ionospheric irregularities observed by SuperDARN radars. *J. Geophys. Res.*, **118**, pp. 5244-5254, https://doi.org/10.1002/jgra.50475.

LIST OF ACRONYMS

AACGM	Altitude Adjusted Corrected Geomagnetic Coordinates
AFRL	Air Force Research Laboratory
AFSPC	Air Force Space Command
CVE	Christmas Valley East (radar)
CVW	Christmas Valley West (radar)
FHE	Fort Hays East (radar)
FHW	Fort Hays West (radar)
GS	Ground Scatter
IRI	International Reference Ionosphere
IS	Irregularity Scatter
LOS	Line-Of-Sight
OTH	Over-The-Horizon
SAPS	SubAuroral Polarization Stream
SuperDARN	Super Dual Auroral Radar Network

DISTRIBUTION LIST

DTIC/OCP
8725 John J. Kingman Rd, Suite 0944
Ft Belvoir, VA 22060-6218 1 cy

AFRL/RVIL
Kirtland AFB, NM 87117-5776 1 cy

Official Record Copy
AFRL/RVB/Leonard M. Berman 1 cy